SI Appendix

H1N1 influenza virus induces narcolepsy-like sleep disruption and targets sleep-wake regulatory neurons in mice

Chiara Tesoriero[a,b,1], Alina Codita[c,1], Ming-Dong Zhang[a,d,1], Andrij Cherninsky[e], Håkan Karlsson[a], Gigliola Grassi-Zucconi[b], Giuseppe Bertini[b], Tibor Harkany[d,f], Karl Ljungberg[g], Peter Liljeström[g], Tomas Hökfelt[a,2], Marina Bentivoglio[b] and Krister Kristensson[a,2]

[a]Department of Neuroscience, Karolinska Institutet, Stockholm SE-17177, Sweden; [b]Department of Neurological and Movement Sciences, University of Verona, Verona 37134, Italy; [c]Department of Neurobiology, Care Sciences and Society, Section of Neurogeriatrics, Karolinska Institutet, Huddinge 14157, Sweden; [d]Division of Molecular Neurobiology, Department of Medical Biochemistry and Biophysics, Karolinska Institutet, Stockholm SE-17177, Sweden; [e]Department of brain physiology, Institute of biology of Taras Shevchenko National University, Kiev 01601, Ukraine; [f]Department of Molecular Neurosciences, Center for Brain Research, Medical University of Vienna, Vienna A-1090, Austria; [g]Department of Microbiology, Tumor and Cell Biology, Karolinska Institutet, Stockholm, Sweden.

[1]These authors contributed equally to the work.

[2]To whom Correspondence may be addressed.

Email: tomas.hokfelt@ki.se or krister.kristensson@ki.se

Materials and Methods

Animals. Female, 3-5 month-old mice knockout for the recombination activating gene 1 (*Rag1*$^{-/-}$; background strain C57BL/6J) were used. Briefly, targeted *Rag1* deletion causes the arrest of rearrangement of B cell receptors (immunoglobulin production) and T cell receptors and absence of T and B cell differentiation, and therefore of adaptive immunity (1). These mice also have high levels of NK-cell activity. The mice derived from the breeding facility at the Department of Microbiology, Tumor and Cell Biology (MTC) of Karolinska Institutet and were maintained in the same animal facility. All experiments were carried out in a BSL2 laboratory, where the mice were housed in IVC cages (3-5 per cage) under a 12h:12h light:dark cycle (lights on at 6 am, *Zeitgeber* time, ZT, 0) with food pellets and water *ad libitum*. Mice were naive to all kind of handling and exposure when the experiments started. After surgery (see below), the mice were housed individually and assigned to one of the experimental groups. The experiments were approved by the local ethics committee (Stockholms Norra Djurförsöksetiska Nämnd, project N87/12). All efforts were made to minimize animal suffering and to reduce the number of animals used.

Influenza A/WSN/33 virus infection. Since the studies were to be performed in mice and potential neuronal targets in the brain were to be traced, a mouse-neuroadapted influenza A (A/WSN/33) (1.4 X 10^5 plaque forming units) virus (kindly provided by Dr. S. Nakajima, The Institute of Public Health, Tokyo, Japan) was used.The mice were instilled with 4-5 μL of the virus suspension or with 0.01 M phosphate-buffered saline, pH 7.4 (PBS) into one nostril for immunohistochemistry or PCR only and into both nostrils for EEG recordings combined with immunohistochemistry or PCR. Previously we have found that intranasal instillation of WSN/33 in small volumes causes a spread to the brain in RAG$^{-/-}$ mice that is not accompanied by virus spread to the lung as determined by PCR (2). This is similar to observations on the highly pathogenic avian influenza A/H5N1 virus in ferrets, which following intranasal viral installation showed viral spread to the brain and not to the lung, but severe bronchointerstitial pneumonia following intratracheal inoculation (3).

For infection, the mice were briefly anaesthetized with isoflurane (Baxter, Deerfield, Illinois, USA). They were then followed daily and sacrificed, together with matched controls, before or when they showed signs of body weight loss, following the institutional guidelines and ethical protocol (see Fig. 1).

Surgery. Surgery was performed to implant wireless NeuroLogger® microchips (NewBehavior, TSE, Hamburg, Germany) in order to record electroencephalography (EEG) as well as body movement (actimetry) via a built-in accelerometer. Six infected mice and 5 saline-exposed control mice were used for this part of the study. Female mice were used to preserve the NeuroLogger device, since they show less social aggressive behavior than male mice. The animals were anesthetized with isoflurane (induction 3% vol/vol, maintenance 1.5-2% vol/vol) and fixed in a stereotactic apparatus (D. Kopf Instruments, Tujunga, CA, USA). The skull was exposed and 3 gold-plated brass screws were inserted into bole holes and served as electrodes: 2 for epidural EEG recording (1.5 mm caudal and 1 mm lateral to bregma; 2.3 mm caudal and 1.7 lateral to bregma, respectively) and a reference electrode (superficial to the cerebellum). Coordinates according to the mouse brain atlas by Franklin and Paxinos (4). To record postural muscle activity in addition to the actimetry signal, in some mice copper wires were implanted in the dorsal neck musculature to record electromyography (EMG). All electrodes leads were soldered to a 7-pin male pitch single row connector, which was fixed to the skull with dental cement (Paladur, Heraeus Kulzer GmbH, Wehrheim, Germany). After surgery, the animals were warmed with an infrared lamp and monitored until they woke up. The animals received acetaminophen (GlaxoSmithKline, Brentford, UK) in drinking water (0.24 mg/ml) for the 7 days recovery period after surgery.

EEG recording and analysis. NeuroLoggers were configured using a specialized software (CommSW, NewBehavior, Zurich, Switzerland) and sampled at 199.8 Hz. Following baseline recordings, performed 7 days after surgery, the mice were treated intranasally with saline or infected as mentioned above and recordings were analyzed every week (see Fig. 1).

Data were downloaded off-line to a PC using a USB plug-in "Readout station" and imported into the MatLab format, using a proprietary software (Converter, Newbehavior, Zurich, Switzerland). The analyses were performed blindly to the animal group assignment. Sleep-wake states were identified using the MatLab software (The MathWorks, Natick, MA, USA). EEG, actimetry signals and EMG were visually scored for 10 s epochs as wakefulness, SWS and REM sleep, according to standard criteria in rodents (5, 6). SOREM episodes were defined as at least 10 s-long REM sleep events preceded by at least 40 s of wakefulness (7). The total time spent in each state (wake, SWS, REM sleep), the number of state episodes, the mean duration of each state episode, the number of sleep-wake transitions and the mean REM sleep latency were calculated for a period of 4 h during the light phase (starting from ZT2-

ZT6, with matched animals of the infected and control groups) and the dark phase (starting from ZT14). The mean REM sleep latency was calculated by averaging the time spent from the beginning of a continuous SWS episode to the beginning of the subsequent REM sleep episode. Cycles lacking REM sleep were considered incomplete and excluded from the calculation. Only ≥ 20 s-long SWS episodes were included in the analysis, thus excluding cycles with SWS episodes shorter than 20 sec.

For spectral analysis, EEG of each vigilance state was analysed separately and epochs containing artefacts were excluded by a semi-automatic algorithm based on amplitude. Spectral analysis of the EEG was performed using Welch method (Matlab, The MathWorks) with a frequency resolution 0.5Hz. Power spectra densities in the 1-25Hz range were analysed. Integral power of EEG in delta (1-5Hz), theta (5.5-10Hz), alpha (10.5-13Hz) and beta (13.5-25Hz) bands were calculated. Data were normalized by division of the band's power to integral spectral power in the 1-25Hz band.

Quantitative real-time RT-PCR. Eleven infected mice (including 4 with EEG recordings) and 7 control mice (including 3 with EEG recordings) were sacrificed by cervical dislocation 26-41 p.i. as indicated in Fig 1. The brain was rapidly dissected out and, after removal of the olfactory bulbs, frozen on dry-ice and stored at -70°C. Total RNA was extracted using the RNeasy kit (Qiagen, Hilden, Germany). The amount and purity of the RNA was assessed by spectrophotometry (PicoDrop Limited, City, UK). Total RNA (1000 ng) was treated with 1 U of amplification-grade DNase I (Invitrogen, Carlsbad, CA, USA) according to instructions from the manufacturer. The DNase-treated RNA was subsequently reverse-transcribed using random hexamers and Super-script II reagents (Invitrogen) according to instructions from the manufacturer.

cDNA templates (1 µl) were amplified in triplicate 25 µl reaction mixtures containing Platinum SYBR Green qPCR Supermix uracil DNA glycosylase (Invitrogen) reagents and 1 µM gene-specific forward and reverse primers ordered from Invitrogen (Table S1). All assays were run on an ABI Prism 7000 real-time thermocycler (Applied Biosystems, Palo Alto, CA, USA). The levels of target transcripts were normalized to those of transcripts encoding hypoxanthine guanine phosphoribosyl transferase (HPRT). From these values, relative differences between the two groups were calculated using the $2^{-\Delta\Delta Ct}$ method (8).

Immunohistochemistry. Intranasally infected (n = 15, including mice with EEG recordings, 2 at 15 days p.i. and 2 at 28-29 days p.i), and non-infected Rag-1$^{-/-}$ mice (n = 5) were deeply anesthetized with sodium pentobarbital (50 mg/kg, i.p., APL, Stockholm, Sweden), and perfused transcardially with 4% paraformaldehyde (wt/vol) with picric acid as previously described (9). Brains, trigeminal ganglia and lungs were dissected out and post-fixed in the same fixative for 90 min at 4°C, followed by rinsing in 10% sucrose (wt/vol) in 0.1M phosphate buffer, pH 7.4, containing 0.01% sodium azide (Merck) and 0.02% bacitracin (Sigma). The tissues were kept in 10% sucrose solution for 2 days at 4°C, and then frozen with liquid carbon dioxide and sectioned on a cryostat (Microm, Heidelberg, Germany). Serial coronal sections were collected at 12 μm thickness for trigeminal ganglia, and 20 μm for brains and lung. The sections were mounted onto superfrost plus microscope slides (Thermo Scientific) and stored at -20°C.

For immunohistochemical processing, sections were dried at room temperature (RT) for at least 30 min and then incubated with rabbit polyclonal antibody against influenza A/WSN/33 virus, diluted 1:100,000 in PBS containing 0.2% (wt/vol) bovine serum albumin (Sigma) and 0.03% Triton X-100 (Sigma) and incubated in a humid chamber at 4°C for 48 h. Immunoreactivities were visualized using the TSA Plus kit (PerkinElmer, Waltham, MA) as previously described (10), except for secondary antibody incubation for 1 h at RT instead of 30 min. For double labeling, TSA Plus staining was first performed followed by the indirect Coons procedure. After the TSA plus staining, sections (without DABCO-mounting) were rinsed in PBS for 30 min and incubated for 48 h at 4°C with primary antibodies (listed in Supplementary Table S2). The sections were first washed with PBS for 30 min and then incubated at RT for 2 h with Cy3-conjugated affinity-purified donkey anti-rabbit IgG (or mixed with donkey anti-guinea pig Cy5, 1:150; Jackson Immunoresearch Laboratories, West Grove, PA), and after rinsing, mounted in DABCO medium. In some cases, counter-staining with DAPI (1:10,000 for 15 min, Sigma) was also added before mounting with DABCO medium.

Imaging and analysis. The material was examined with an LSM700 confocal laser-scanning microscope (Zeiss), and images acquired from one airy unit pinhole as previously described (10). Emission spectra for each dye were limited as follows: FITC or Alexa Fluro488 (505–540 nm), Cy3 (560–610 nm), Cy5 (>610 nm) and DAPI (420-460 nm). For the overview of influenza A/WSN/33 virus staining from brain sections, tile scan module together with 5X

objective was applied. Projection pictures were acquired from orthogonal z-stack with a depth interval of 1.0 μm with the 40X water objective (N.A. 1.40). Images were processed using the ZEN2012 software (Zeiss). Multi-panel figures were assembled in Adobe Photoshop CS6 software (Adobe System).

For quantification of loss of Orx/Hcrt- and MCH-positive neurons in lateral hypothalamus, *Rag1*$^{-/-}$ mice (n=4) with unilateral influenza A virus infection were included. Two to four sections from lateral hypothalamus per mouse (similar levels) labeled with Orx/Hcrt or MCH antibodies were selected and scanned with confocal microscope (10X, tile scan). Orx/Hcrt- and MCH-positive neurons were counted using ZEN2012 software manually. The loss of Orx/Hcrt- and MCH-positive neurons was calculated by comparing with the contralateral, uninfected side. The cell loss ratio is presented as mean ± SEM (standard error of mean).

Statistics. At the time of infection mice from the same original home-cage were assigned to the two experimental groups.

The distribution of the data was assessed using Shapiro-Wilk, whereas the homogeneity of variance was assessed using the Levene's test. Statistical analyses were performed using SPSS (Chicago, Illinois, USA). For the EEG data, comparisons between the infected and saline-treated groups were carried out using the non-parametric Mann-Whitney test. To investigate changes over time, we used the Linear Mixed Model, which enables longitudinal analysis with missing data. Model fit improvement was assessed using the Akaike's information criterion. For the spectral power data, comparisons between the experimental groups were carried out using the non-parametric Kruskal-Wallis test. For RT-PCR data, comparisons between the infected and saline-treated groups were evaluated by the non-parametric Mann-Whitney test. A Spearman's rank-order correlation was run to determine whether a relationship could be found between percentage of body weight loss and the total number of sleep-wake transitions during both light and dark phases. This parameter was chosen as the most representative of narcolepsy-like sleep disturbances.

In all analyses, statistical significance was set at $p < 0.05$.

1. Mombaerts P*, et al.* (1992) RAG-1-deficient mice have no mature B and T lymphocytes. *Cell* 68(5):869-877.
2. Aronsson F, Robertson B, Ljunggren HG, & Kristensson K (2003) Invasion and persistence of the neuroadapted influenza virus A/WSN/33 in the mouse olfactory system. *Viral immunology* 16(3):415-423.

3. Bodewes R*, et al.* (2011) Pathogenesis of Influenza A/H5N1 virus infection in ferrets differs between intranasal and intratracheal routes of inoculation. *The American journal of pathology* 179(1):30-36.
4. Franklin KBJ & Paxinos G (2008) *The mouse brain in stereotaxic coordinates* (London : Elsevier/Academic Press, New York, N.Y.) 3rd compact Ed.
5. Radulovacki M, Virus RM, Djuricic-Nedelson M, & Green RD (1984) Adenosine analogs and sleep in rats. *The Journal of pharmacology and experimental therapeutics* 228(2):268-274.
6. Tobler I, Deboer T, & Fischer M (1997) Sleep and sleep regulation in normal and prion protein-deficient mice. *The Journal of neuroscience : the official journal of the Society for Neuroscience* 17(5):1869-1879.
7. Scammell TE, Willie JT, Guilleminault C, Siegel JM, & International Working Group on Rodent Models of N (2009) A consensus definition of cataplexy in mouse models of narcolepsy. *Sleep* 32(1):111-116.
8. Livak KJ & Schmittgen TD (2001) Analysis of relative gene expression data using real-time quantitative PCR and the 2(-Delta Delta C(T)) Method. *Methods* 25(4):402-408.
9. Shi TJ*, et al.* (2012) Secretagogin is expressed in sensory CGRP neurons and in spinal cord of mouse and complements other calcium-binding proteins, with a note on rat and human. *Molecular pain* 8:80.
10. Zhang MD*, et al.* (2014) Neuronal calcium-binding proteins 1/2 localize to dorsal root ganglia and excitatory spinal neurons and are regulated by nerve injury. *Proceedings of the National Academy of Sciences of the United States of America* 111(12):E1149-1158.

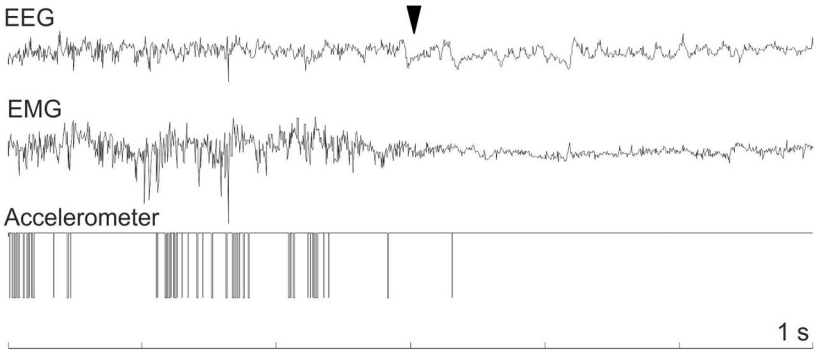

Fig. S1. Electroencephalogram (EEG), electromyogram (EMG) and accelerometric traces (1 s epochs) of a sleep-onset REM sleep (SOREM) episode recorded in an infected mouse during the 4th week p.i. (w4). The arrowhead points to the direct transition from W to REM sleep, characterized by EEG traces similar to W, but with the sudden loss of skeletal muscle tone and behavioral immobility.

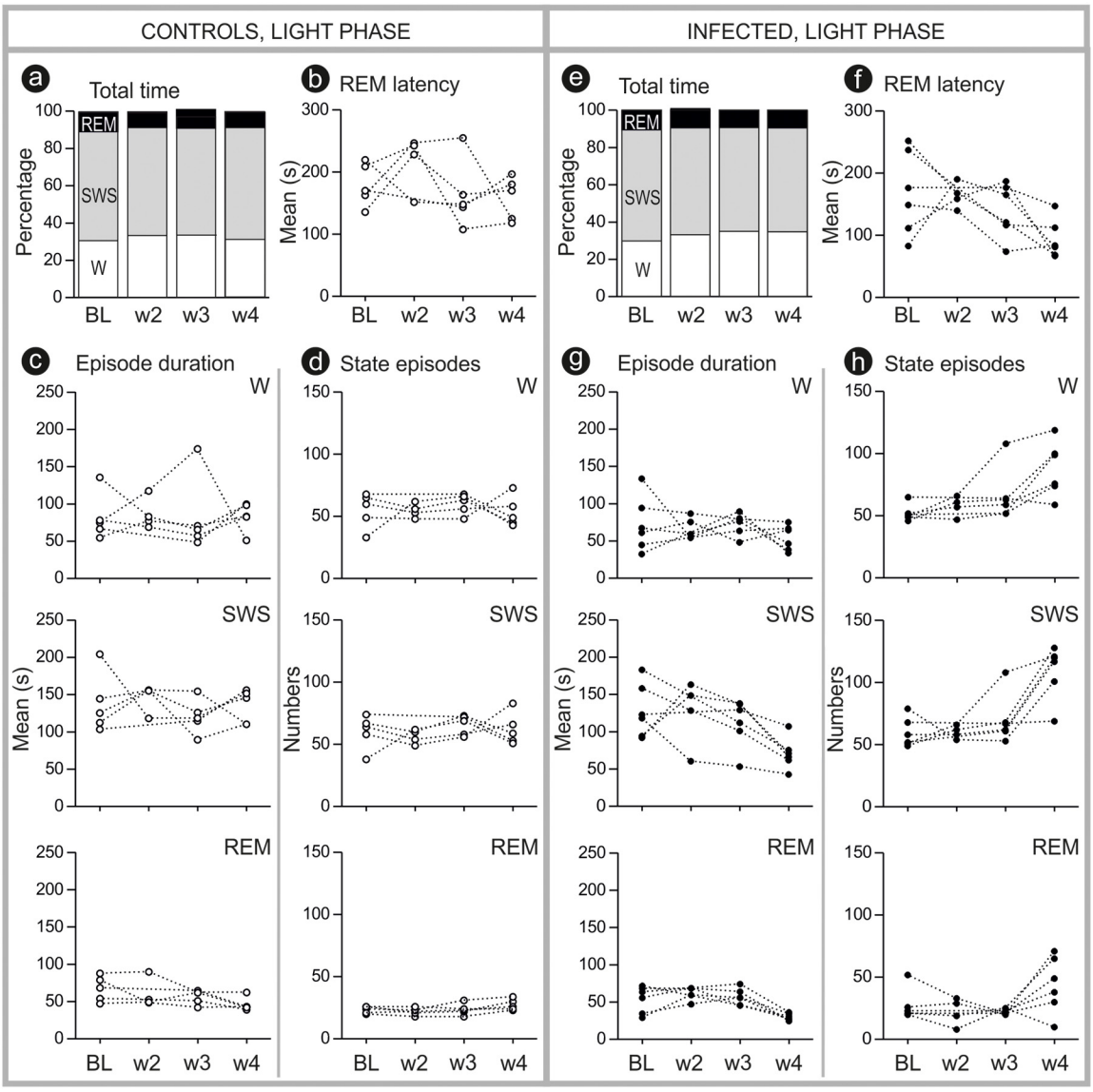

i

Exposure	N. of mice	Recording	% Total time W		% Total time SWS		% Total time REM		Episode duration (s) W		Episode duration (s) SWS		Episode duration (s) REM		State Episodes (n) W		State Episodes (n) SWS		State Episodes (n) REM		SOREM episodes		Mean REM latency (s)	
Virus	6	BL	27	(18)	61	(18)	11	(3)	65	(62)	121	(71)	60	(36)	50	(7)	55	(20)	22	(12)	0	(0)	163	(137)
Virus	4	w2	29	(23)	60	(19)	11	(5)	67	(29)	139	(82)	64	(18)	59	(15)	60	(10)	24	(21)	0	(0)	163	(40)
Virus	6	w3	35	(7)	56	(9)	9	(3)	78	(23)	121	(48)	56	(21)	61	(23)	65	(19)	22	(4)	0	(0)	143	(73)
Virus	6	w4	30	(19)	59	(17)	10	(6)	56	(32)	69	(26)	30	(9)	88	(35)	119	(30)	44	(42)	1	(2)	83	(53)
Saline	5	BL	33	(9)	58	(5)	11	(5)	75	(46)	125	(66)	69	(33)	60	(26)	64	(23)	24	(6)	0	(0)	170	(65)
Saline	4	w2	33	(12)	56	(10)	9	(3)	80	(38)	155	(29)	51	(32)	55	(11)	57	(11)	22	(7)	0	(0)	236	(75)
Saline	5	w3	28	(19)	63	(17)	11	(4)	66	(69)	119	(38)	62	(17)	63	(15)	69	(16)	23	(8)	0	(0)	148	(84)
Saline	5	w4	33	(8)	60	(8)	9	(2)	84	(32)	146	(43)	43	(12)	49	(22)	59	(23)	26	(9)	0	(0)	170	(67)

Fig. S2. Sleep-wake pattern of infected vs. control mice, during the light phase, over the course of 4 weeks. (a, e) The stacked-bar charts show the fraction of time spent in the different vigilance states at the 4 studied time points. In all the other charts, the lines represent individual animals. (b, f) Mean duration of slow wave sleep (SWS) phases immediately preceding rapid eye movement (REM) sleep (see text for more details). (c, g) Mean duration of wake (W), SWS, and REM sleep episodes. (d, h) Number of episodes of the same states over the 4 h epoch studied. (i) For each of the analyzed vigilance state parameters, and for each experimental group and time point, the Table shows median values accompanied by the interquartile range (in parentheses). No significant changes in the total time spent in each state are recorded in control (a) and infected (e) groups over the course of 4 weeks. However, a decrease of the mean duration of state episodes and an increase of their number are observed in the infected group. Notably, statistical analysis (Linear mixed model) shows a significant interaction time*treatment in the mean duration of SWS ($F=3.752$, $p=0.035$) and in the number of SWS and REM episodes ($F=3.981$, $p=0.047$; $F=6.363$, $p=0.016$, respectively). (i) The Table shows all the raw data (with interquartile range within brackets)

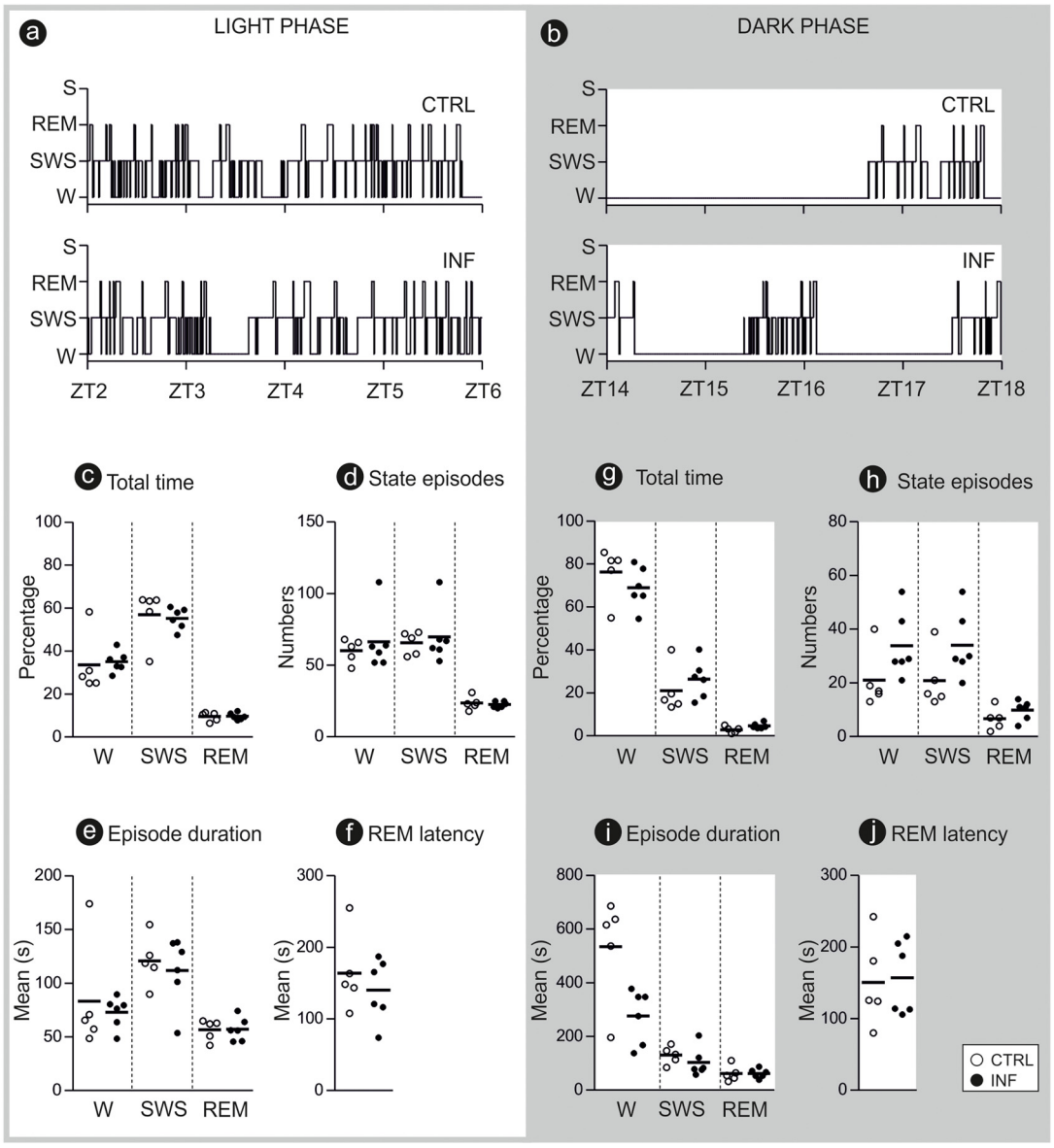

Fig. S3. (a-j) Sleep-wake pattern of infected (INF) mice (n=6) compared to controls (CTRL) mice (n=5) during the 3rd week p.i. (a-b) Representative 4 h hypnograms in the light (a) and dark (b) phases. (c-j) Quantitative data of vigilance state parameters in the light (c-f) and dark (g-j) phases are presented as scatter plots and horizontal lines indicate median values. In both the light and dark phases, infected mice show no significant difference in sleep-wake parameters with respect to control mice (Mann-Whitney test).

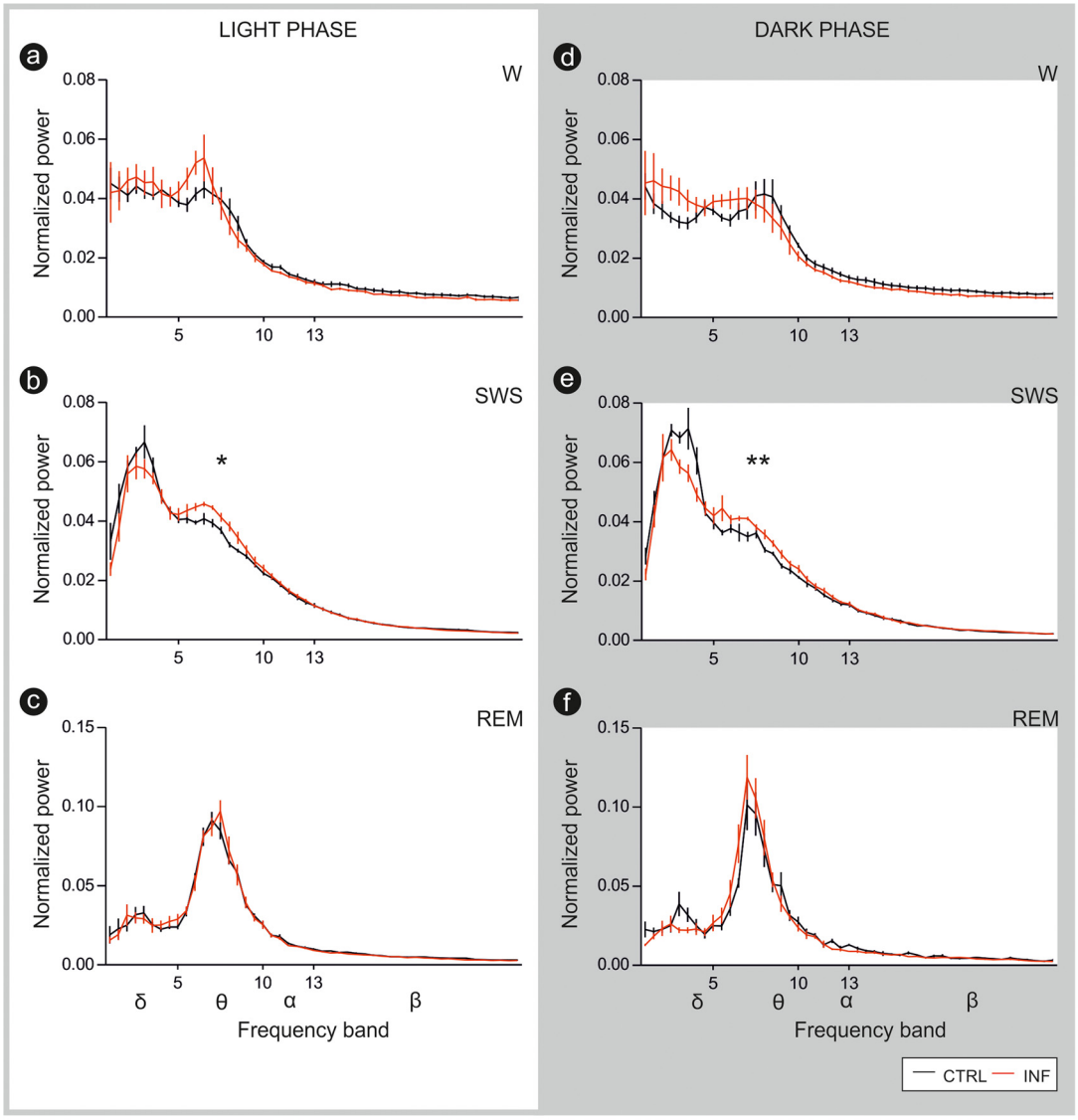

Fig. S4. EEG power spectra during wakefulness (W), slow wave sleep (SWS) and rapid eye movement (REM) sleep in control (CTRL) and infected (INF) mice during the 4th week p.i. (a-f) Similar shapes of the spectral powers (mean +/- SEM) at every stage of W and REM sleep are observed in the two experimental groups (CTRL n=5; INF n=5) during both the light and dark phases. Compared to the control group, infected mice show a significant increase in the theta band power of the SWS during both the light (b) ($H(1) = 4.811$, $p=0.032$) and dark (e) ($H(1) = 5.771$, $p=0.016$) phases (Kruskal-Wallis test, *$p<0.05$, **$p<0.01$).

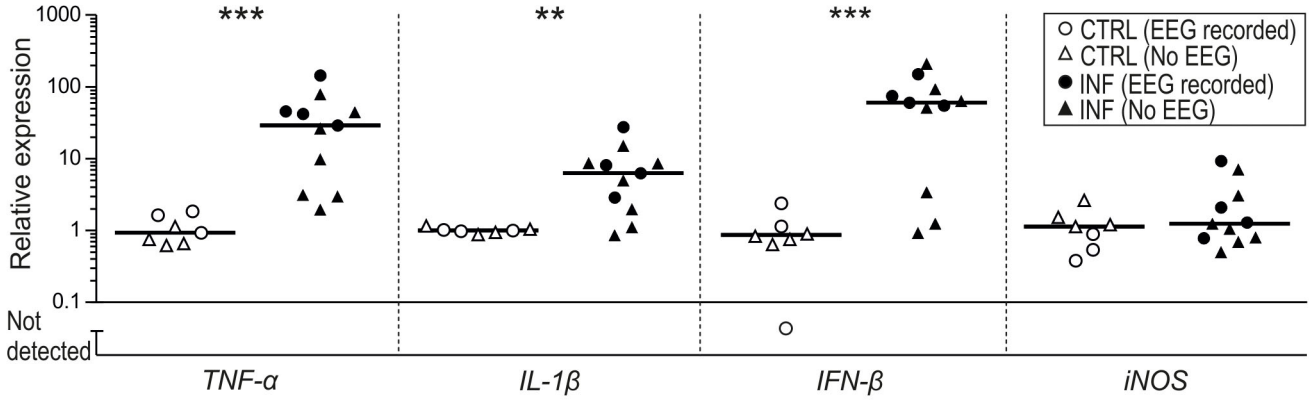

Fig. S5. Transcripts encoding pro-inflammatory molecules. Relative levels of transcripts observed at 3-7 weeks after intranasal instillation of influenza A/WSN/33 virus (n=11, including 4 mice with recording of neurophysiological parameters, indicated as EEG) or vehicle (CTRL, n=7, including 3 mice with EEG recording). Dots represent individual mice, horizontal lines indicate median values (Mann-Whitney test, **p<0.01, ***p<0.001). Transcripts encoding tumor necrosis factor-α (TNF-α) (Ws=28.00, p=0.0001), interleukin-1β (IL-1β) (Ws=36.00, p=0.0041) and interferon-β (IFN-β) (Ws=31.00, p=0.0004) are highly significantly increased in the infected group, whereas the level of the transcript encoding inducible nitric oxide synthase (iNOS) is similar in the infected and control groups. Note that in the control mice, in which EEG was recorded, pro-inflammatory cytokine transcript expression does not increase, indicating that the EEG recording procedure per se does not cause inflammatory changes.

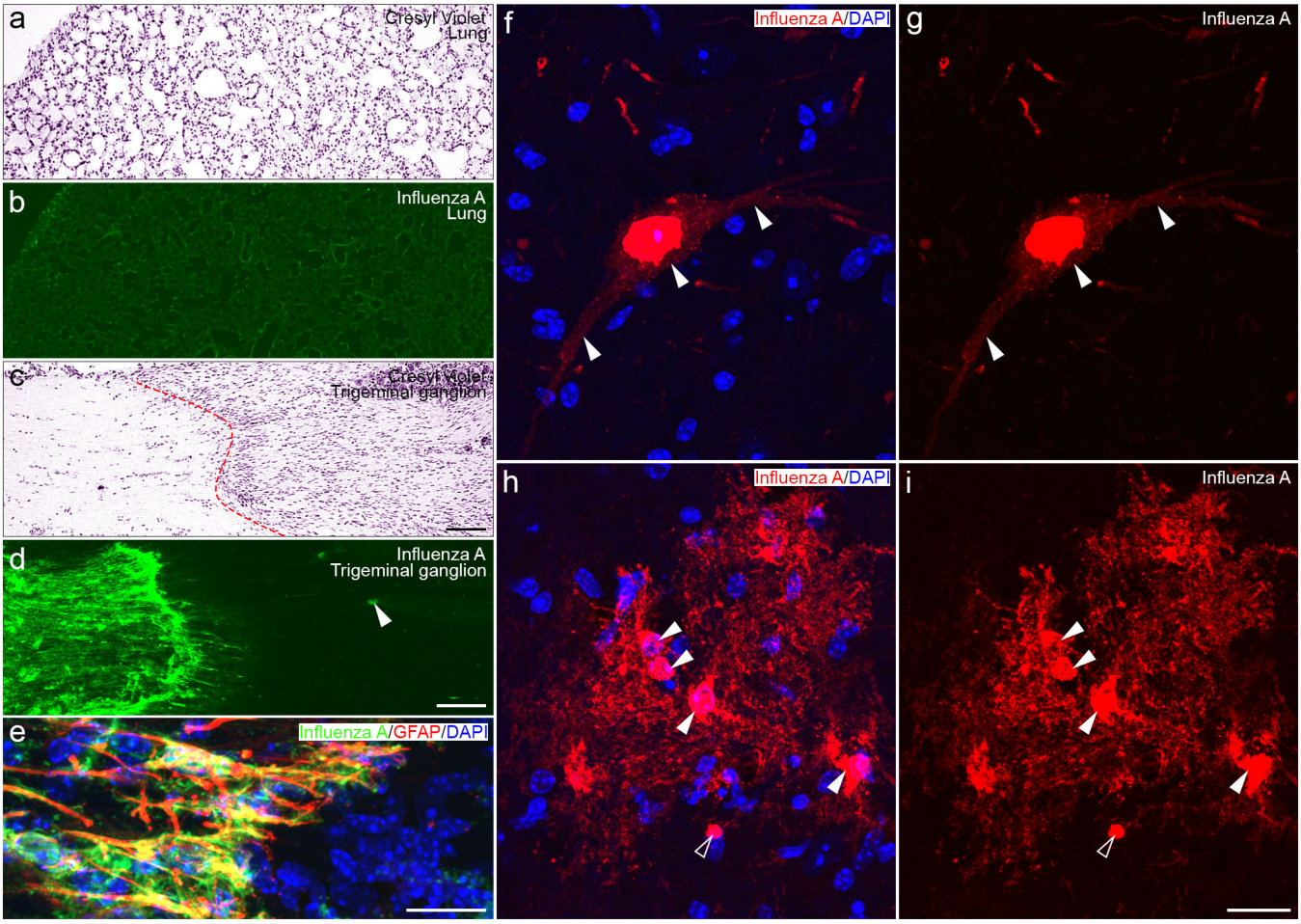

Fig. S6. Viral antigens in trigeminal nerve and brain stem. (a, b) Viral antigen can not be detected in lung. Adjacent section stained with cresyl violet. (c-e) In the trigeminal ganglion viral antigen can only be detected in few neurons (arrowhead, d), sharply contrasting the strong labelling of the nerve (d) proximal to the border between central and peripheral nervous system (red line, c, cresyl violet). Triple labelling shows presence in astrocytes (e; 16 µm thickness z-stack scanning 1 µm interval. (f,g) Viral antigen in brain stem neuron with strong nuclear and weak cytoplasmic staining (18 µm thickness, z-stack scanning). (h,i) Viral antigens (red) in brain stem microglia with ramified branches (arrowheads) and astrocyte (staining only nucleus, open arrowhead) (DAPI, blue) (12 µm thickness, z-stack scanning). (For details see Fig. S8 and S9 for double labelling with Iba1 or GFAP.) Scale bars: 100 µm in a,c; 200 µm in b,d; 10 µm in e,i.

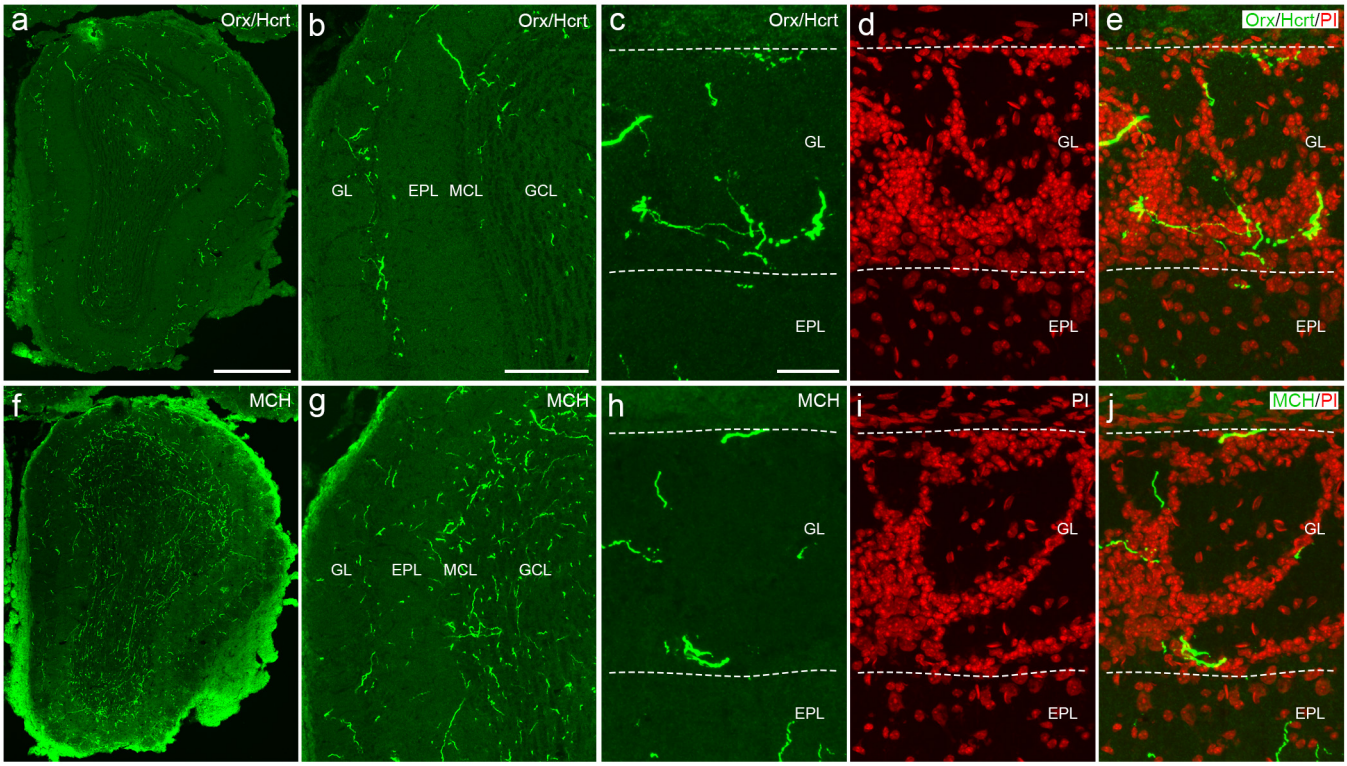

Fig. S7. Orx/Hcrt and MCH innervation of the olfactory bulb. (a) Overview of Orx/Hcrt-IR fibers. (b) Orx/Hcrt-IR fibers mainly distribute to the glomerular (GL) and granule cell layers (GCL). (c-e) High magnification of Orx/Hcrt-IR fibers innervating the GL. (f) Overview of MCH-IR fibers. (g) MCH-IR fibers mainly distribute to GCL and extend to GL. (h-j) High magnification of MCH-IR fibers innervating the GL. Dashed lines lindicate borders between the olfactory nerve layer, GL and external plexiform layer (EPL). MCL: mitral cell layer. Scale bars: 500 μm in a and f, 200 μm in b and g, 50 μm in c-e and h-j.

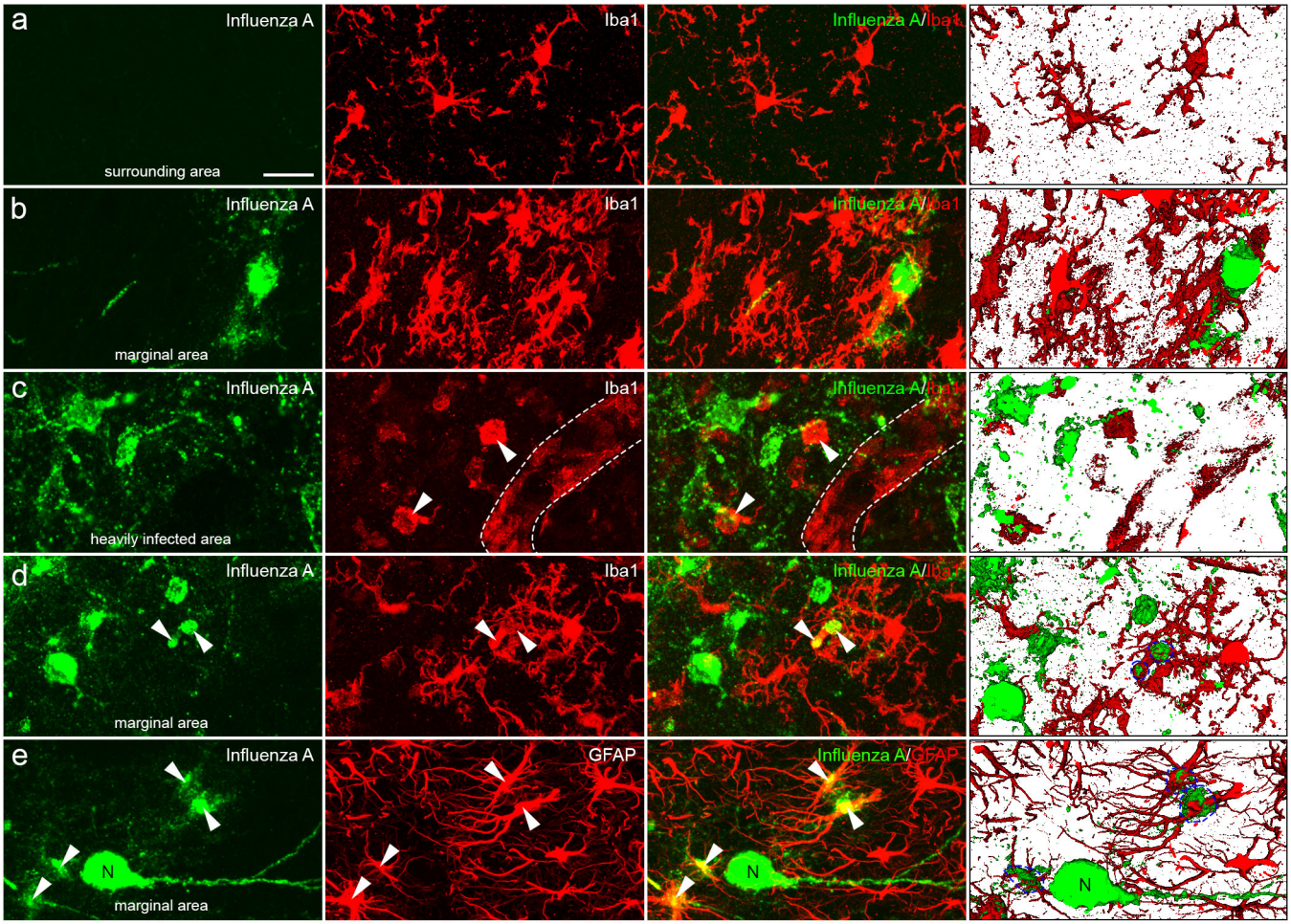

Fig. S8. Virus-induced activation of, especially, microglia in lateral hypothalamus. (a) Resting microglia labeled with Iba1 in area surrounding virus-infected patch, being similar to control conditions. (b) Activated microglia with thick ramified branches in the marginal zone bordering to the heavily infected area. (c) In the latter area, with cell death, Iba1 labels amoeboid form of microglia (macrophage, arrowheads) close to blood vessel (dashed lines; perivascular macrophage). (d) A few cases of Iba1-labeled microglia co-localized with viral antigens in the marginal area. (e) Many GFAP-labeled astrocytes are positive for viral antigens. Arrowheads in (d) and (e) indicate co-localization. The right, outer column of a-d, respectively, shows surface 3D structure, to facilitate recognition of glia cell shape and co-localization. Z-stack scanning 1 µm interval from 14 µm- (a,c) and 18 µm-(d,e) thick tissue. Scale bar: 20 µm.

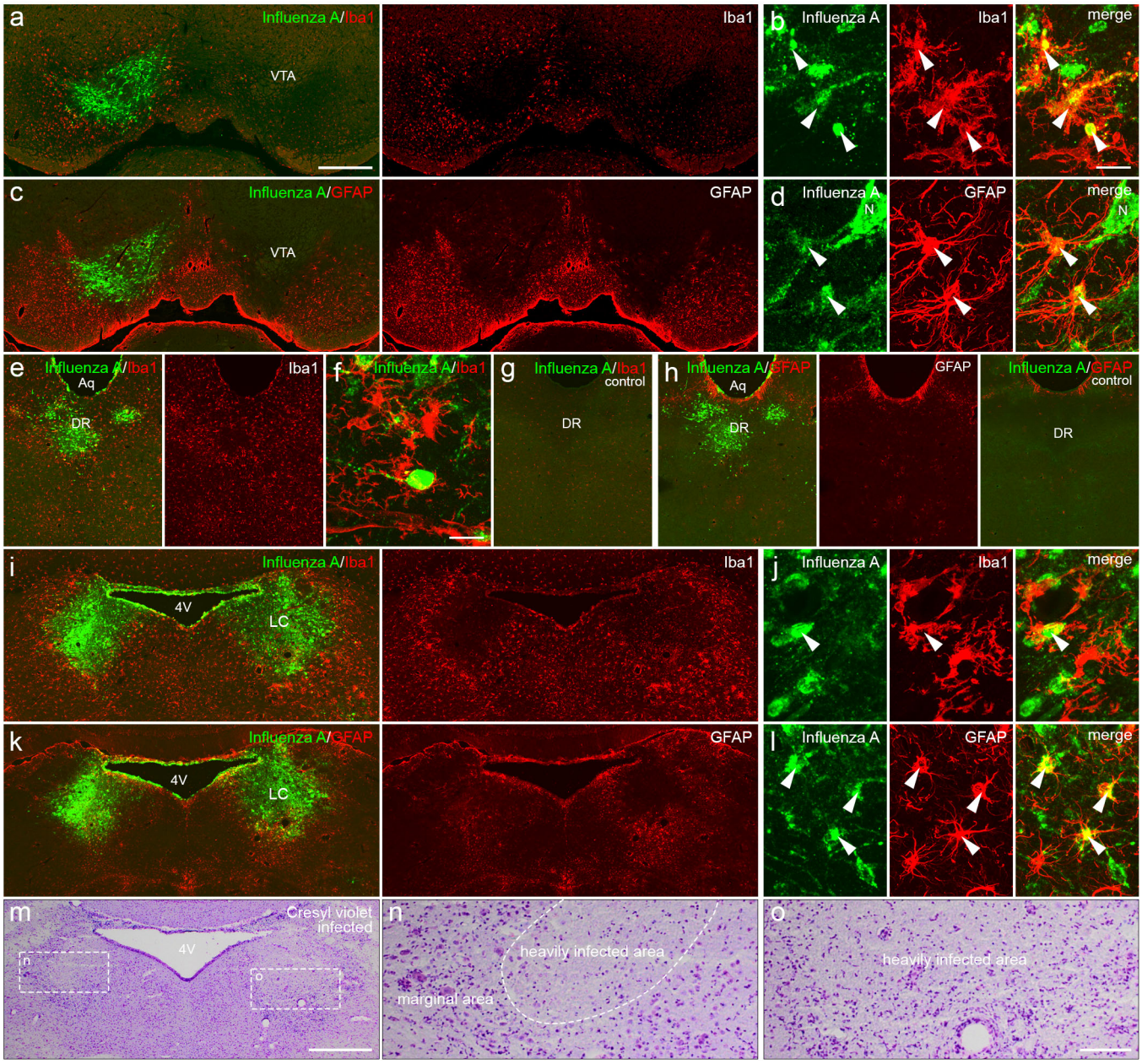

Fig. S9. Activated glia in further areas involved in sleep-wake regulation. (a-d) Activated microglia (a,b) and astrocytes (c,d) in the ventral tegmental area (VTA). Both types of glia harbor viral antigens as indicated by arrowheads. (e-h) In dorsal raphe (DR), there is an increase in microglia, often with thick branches, surrounding the virus patch, although virus-Iba1 co-localization is rare/cannot be detected. Astrocyte activation is not prominent. (i-l) Locus coeruleus (LC) displays activated microglia (i) and astrocytes (k). Many astrocytes harbor viral antigens (arrowheads) in the marginal area (l), whereas most microglia do not (j, only a single cell encountered). Many Iba1-positive cells are seen within the heavily infected area on both sides (i, right side). (m-o) Cresyl violet staining of adjacent section reveals cell loss with only a few preserved cells left in heavily infected areas mainly within the LC. Cells in the marginal area (mesencephalic trigeminal nucleus and pontine central gray) still appear intact (n). Macrophages in the heavily infected area are also seen (o). High magnification co-localization photomicrographs from VTA (11 µm-) and DR and LC (12 µm- thick z-stack). Scale Bars: 500 µm in a,c,e,g-k,m; 20 µm in b,d,j,l; 10 µm in f, 100 µm in n,o.

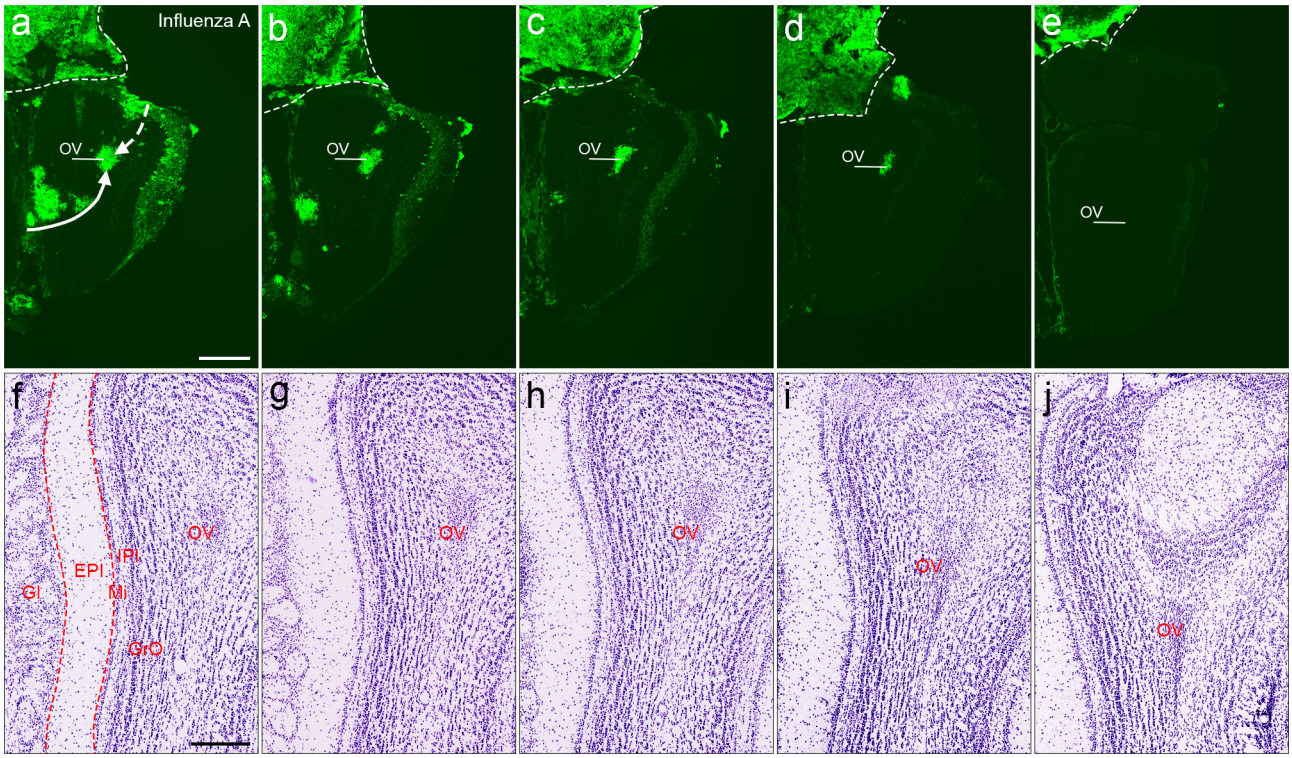

Fig. S10. Viral antigens spreading into olfactory ventricule (mouse #6). (a-e) Viral antigens form patches in olfactory nerve layer and extend into the granule cell layer GrO), and are also seen in olfactory ventricle (OV) (a) and fibers in external plexiform (EPl) and mitral cell (Mi) layers are labelled (sections from rostral to caudal). Viral antigens remain in the ventricle (a-d) and disappear caudally (e). Arrows indicate possible viral migration paths to OV. (f-j) Cresyl violet staining of adjacent sections. Gl, glomerular layer; IPl, interal plexiform layer. Scale bars: 500 µm in a-e; 200 µm in f-j.

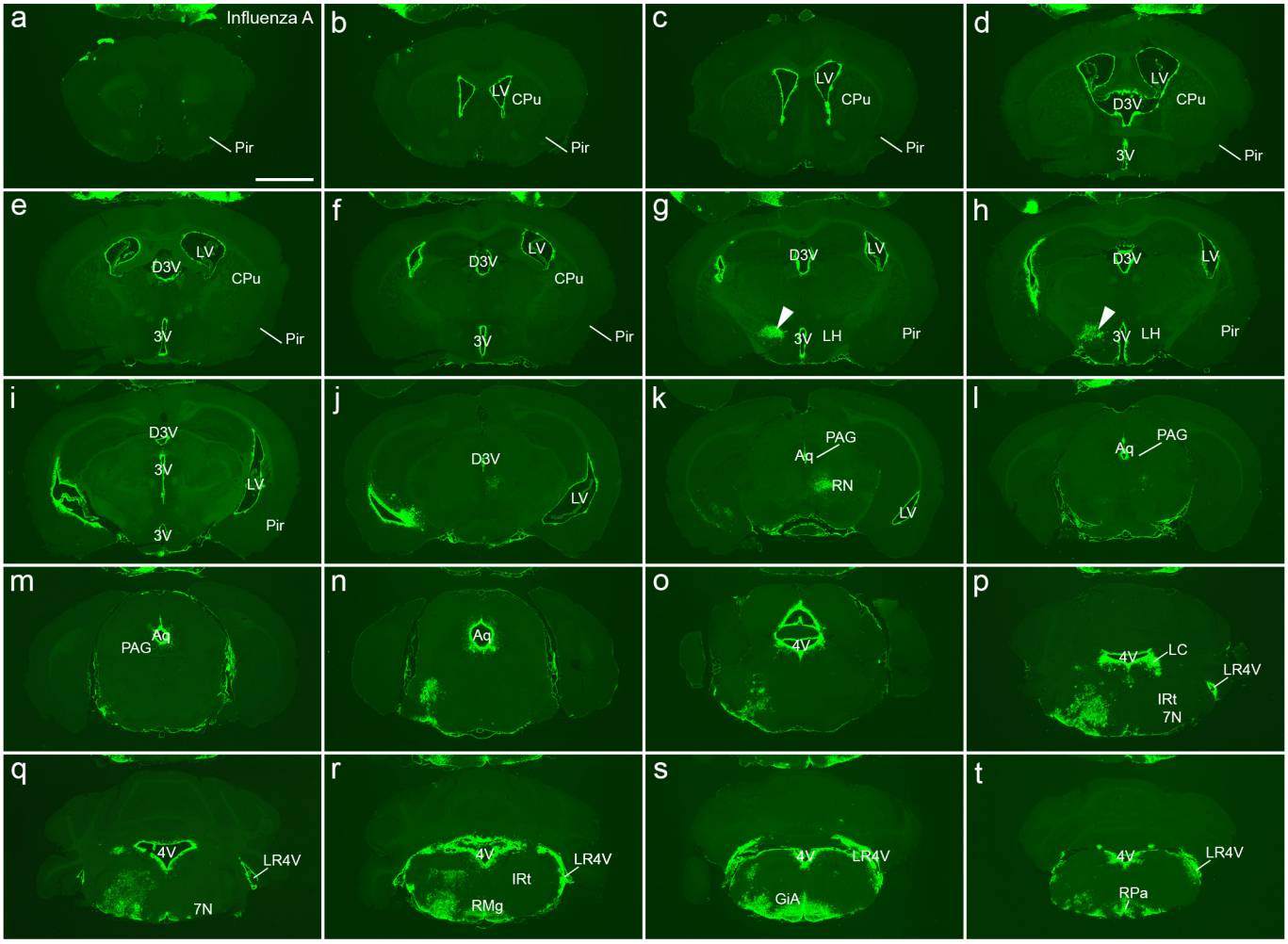

Fig. S11. Overview of distribution of viral antigens in the brain (mouse #6). (a-t) Parenchymal labeling is mainly unilateral, and also the ventricular labeling is stronger on that side, the red nucleus (RN) being an exception. (a-f) Throughout the rostral forebrain the infection is only found along the ventricular system, continuing to the medulla oblongata (g-t). (g, h) A unilateral virus infection is seen in the lateral hypothalamus (LH) (arrows). From this level and caudally there is a labeling along the ventral meninges (g-t). (m,n) Spread of virus into the periaqueductal gray (PAG), including the most dorsal aspects of the dorsal raphe. (n-t) From the mid-pontine level there is a unilateral column along the ventro-lateral aspects of the pons and medulla oblongata including the trigeminal and facial nerve territories, such as the reticular nuclei, although less dramatic as compared to mouse #1 (Figure 4). (p) In pons, virus invasion appear to extend from the ventricular surface into the locus coeruleus region (LC), some noradrenaline neurons in the dorsal aspects being labeled. However, small patches of virus are also seen throughout the entire nucleus. Other areas infected include gigantocellular reticular nucleus, pars alpha (GiA), nucleus raphe pallidus (RPa), the inferior olive and nucleus raphe magnus (RMg). 3V, 3rd ventricle; 4V, 4th ventricle; 7N, facial nucleus;Pir, piriform cortex; Aq, Aqueduct; CPu, caudate putamen; D3V, dorsal 3rd ventricle; IRt, intermediate reticular nucleus;tuberomammilary nuclei (TMN), LR4V, lateral recess of the 4th ventricle; LV, lateral ventricle; Scale bar: 2 mm

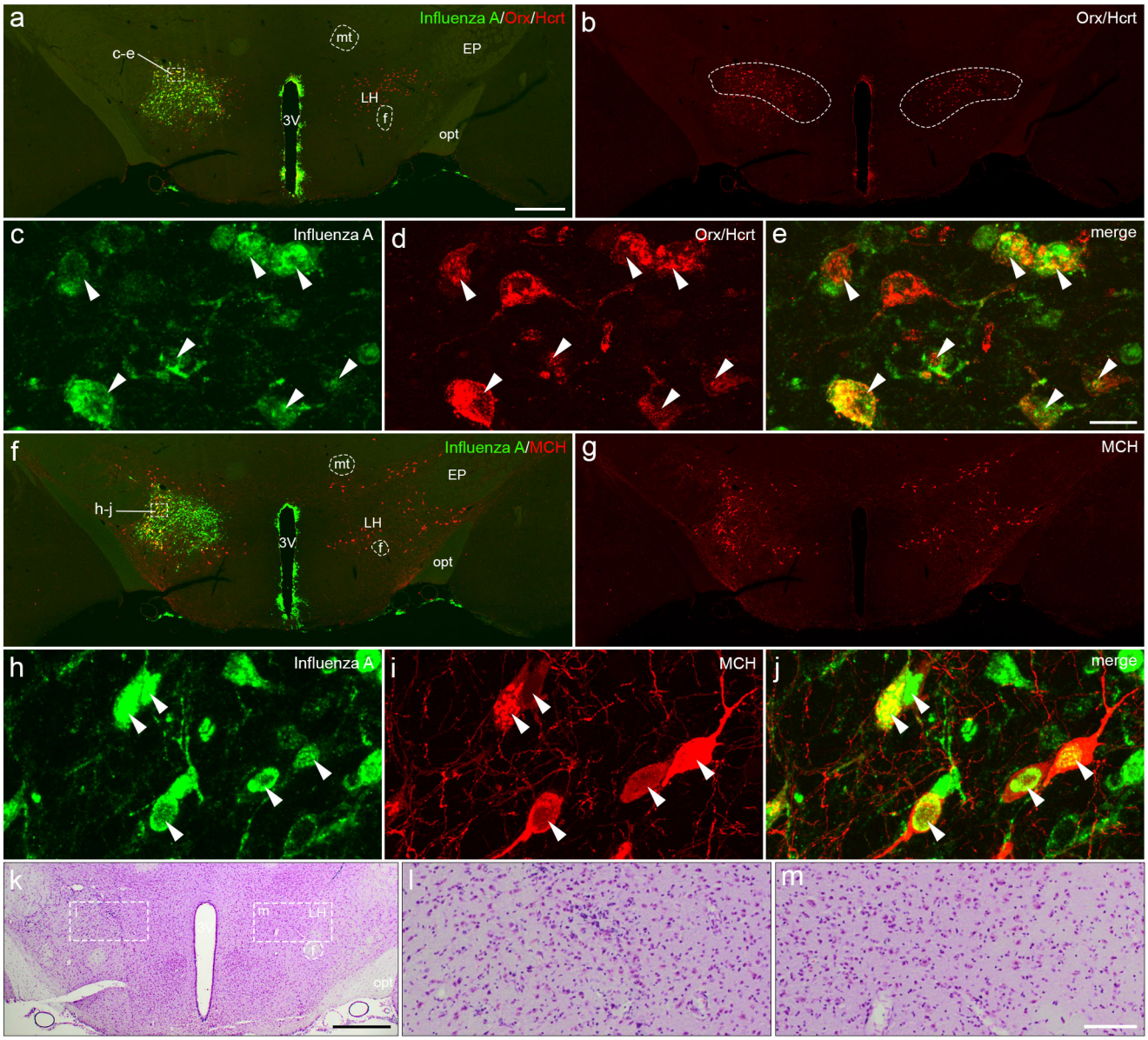

Fig. S12. Viral antigens in Orx/Hcrt and MCH neurons with surrounding activated glial cells (mouse #6). (a-e) In the lateral hypothalamus (LH), the virus targets Orx/Hcrt -positive neurons, although the peptide expression even within the patch is apparently not affected (cf. Fig.5). Arrowheads indicate that most Orx/Hcrt neurons are infected (c-e). (f-j) Virus also infects MCH-positive neurons in LH (arrowheads), especially in the lateral aspects. MCH expression does not appear affected. Note that the MCH neurons have more distinct dendrites and better preserved surrounding nerve terminals than than the Orx/Hcrt neurons. (k-m) No marked differences can be seen between the two sides after cresyl violet staining: Nerve cell bodies are well preserved. Scale bars: 500 µm in a, b, f, g and k, 20 µm in c-e,h-j; 100 µm in l,m.

Table S1. Transcripts analyzed by quantitative real-time RT-PRC

Gene	Forward sequence	Reverse sequence
HPRT	CCCAGCGTCGTGATTAGC	GGAATAAACACTTTTTCCAAATCC
IFNβ	CCATCATGAACAACAGGTGGAT	GAGAGGGCTGTGGTGGAGAA
IL-1β	TGGTGTGTGACGTTCCCATT	CAGCACGAGGCTTTTTTGTTG
i-NOS	CAGCTGGGCTGTACAAACCTT	CATTGAAAGTCAAGCGTTTGC
TNFα	GGCTGCCCCGACTACGT	GACTTTCTCCTGGTATGAGATAGCAAA

Table S2. Primary antibodies used in this study

Antibody	Host	Antigen	Supplier/ Catalog number	Dilution
ChAT	Goat polyclonal	Human placental ChAT	Millipore (Billerica, MA)/AB144P	1:500
GAD67	Mouse monoclonal	Recombinant GAD67	Millipore (Billerica, MA)/MAB406	1:500
GFAP	Rabbit polyclonal	GFAP from Cow spinal cord	DAKO (Glostrup, Denmark)/Z0334	1:1,000
HDC	Rabbit polyclonal	HDC from *E. coli*	American Research Products (Waltham, MA)/03-16045	1:500
Iba1	Rabbit polyclonal	Conserved C-terminal synthetic peptides	Wako (Osaka, Japan)/019-19741	1:500
Influenza A	Rabbit polyclonal	Amino acids 1-308 of haemagglutinin	S. Nakajima (Tokyo, Japan)	1:100,000
MCH	Rabbit polyclonal	Full length MCH peptide	Phoenix Pharmaceuticals (Burlingame, CA)/H-070-47	1:400
Orexin-A	Goat polyclonal	C-terminus of human orexin-A	Santa Cruz (Dallas,TX)/sc-8070	1:2,000
Orexin	Rabbit polyclonal	Rabbit amino acids 114-130 of rat orexin	L. De Lecea (Stanford, CA)	1:400
TH	Rabbit polyclonal	Human native TH	M. Goldstein (New York, NY)	1:800
TPH	Goat polyclonal	Recombinant rabbit tryptophan hydroxylase	Millipore (Billerica, MA)/AB1541	1:800
VGLUT2	Guinea pig polyclonal	C-terminal sequence of mouse VGLUT2 (aa 549-582)	M. Watanabe (Sapporo, Japan)	1:500